Low-Lying Excited States and Primary Photoproducts of $[Os_3(CO)_{10}$-(*s-cis*-L)] (L = Cyclohexa-1,3-diene, Buta-1,3-diene)] Clusters Studied by Picosecond Time-Resolved UV/Vis and IR Spectroscopy and by Density Functional Theory

Frank W. Vergeer,[a] Pavel Matousek,[b] Michael Towrie,[b] Paulo J. Costa,[c, d] Maria J. Calhorda,[c, d] and František Hartl*[a]

Abstract: Combined picosecond transient absorption and time-resolved infrared studies were performed, aimed at characterising low-lying excited states of the cluster $[Os_3(CO)_{10}$(*s-cis*-L)] (L = cyclohexa-1,3-diene, **1**) and monitoring the formation of its photoproducts. Theoretical (DFT and TD-DFT) calculations on the closely related cluster with L = buta-1,3-diene (**2′**) have revealed that the low-lying electronic transitions of these $[Os_3(CO)_{10}$(*s-cis*-1,3-diene)] clusters have a predominant σ(core)π*(CO) character. From the lowest σπ* excited state, cluster **1** undergoes fast Os–Os(1,3-diene) bond cleavage ($\tau = 3.3$ ps) resulting in the formation of a coordinatively unsaturated primary photoproduct (**1a**) with a single CO bridge. A new insight into the structure of the transient has been obtained by DFT calculations. The cleaved Os–Os(1,3-diene) bond is bridged by the donor 1,3-diene ligand, compensating for the electron deficiency at the neighbouring Os centre. Because of the unequal distribution of the electron density in transient **1a**, a second CO bridge is formed in 20 ps in the photoproduct $[Os_3(CO)_8(\mu\text{-}CO)_2$-(cyclohexa-1,3-diene)] (**1b**). The latter compound, absorbing strongly around 630 nm, mainly regenerates the parent cluster with a lifetime of about 100 ns in hexane. Its structure, as suggested by the DFT calculations, again contains the 1,3-diene ligand coordinated in a bridging fashion. Photoproduct **1b** can therefore be assigned as a high-energy coordination isomer of the parent cluster with all Os–Os bonds bridged.

Keywords: cluster compounds · density functional calculations · diene ligands · IR spectroscopy · photochemistry

Introduction

Photochemical and photophysical studies of transition-metal carbonyl clusters are of considerable interest. The reason is not only their potential to act as versatile catalysts or catalyst precursors,[1] in fine chemistry, for example, but also their challenging application as key components of more complex supramolecular systems. The photoactivation of (thermally stable) cluster compounds may lead to novel reactions of high selectivity.[2,3] In tailored supramolecular systems with cluster moieties connecting donor and acceptor sites, changes in the structural and electronic properties of the cluster induced by the light absorption may be utilised in, for example, controlled electron/energy transport.

Time-resolved infrared spectroscopy (TRIR), in which UV-visible flash photolysis is combined with (ultra)fast infrared detection, is a powerful tool for probing the primary events after photoexcitation. This applies especially to complexes containing strongly IR-active ligands, such as CO or NO, which can act as direct IR probes of the electron density at the metal centre. As photoexcited transition-metal

[a] Dr. F. W. Vergeer, Dr. F. Hartl
Institute of Molecular Chemistry
Universiteit van Amsterdam
Nieuwe Achtergracht 166, 1018 WV Amsterdam (The Netherlands)
Fax: (+31) 20-525-6456
E-mail: hartl@science.uva.nl

[b] Dr. P. Matousek, Dr. M. Towrie
Central Laser Facility
CCLRC Rutherford Appleton Laboratory
Chilton, Didcot, Oxfordshire OX11 0QX (United Kingdom)

[c] P. J. Costa, Prof. M. J. Calhorda
Instituto de Tecnologia Química e Biológica
Av. da República, EAN, Apart. 127
2781-901 Oeiras (Portugal)

[d] P. J. Costa, Prof. M. J. Calhorda
Dep. de Química e Bioquímica
Faculdade de Ciências, Universidade de Lisboa
1749-016 Lisboa (Portugal)

Supporting information for this article is available on the WWW under http://www.chemeurj.org/ or from the author.

 DOI: 10.1002/chem.200400086

clusters are usually too short-lived to be studied with nanosecond (ns) transient absorption (TA) or TRIR, faster spectroscopic techniques are required in order to characterise the excited states and to monitor the formation of the primary photoproducts. Although several picosecond (ps) TRIR studies of simple, mononuclear transition-metal complexes with, for example, M^0 (Cr, Mo, W[4] or Fe[5]) and M^I (Co,[6] Rh and Ir[7]) centres have been reported, those of di- and polynuclear transition-metal complexes are scarce.[8] We have recently used ps TRIR conveniently to probe the photoreactions of the triangular clusters $[Ru_3(CO)_{12}]$[9] and $[Ru_3(CO)_8(\mu\text{-}CO)_2(dmb)]$ (dmb = 4,4′-dimethyl-2,2′-bipyridine),[10] in particular by monitoring the spectral changes in the bridging carbonyl region.

$[Ru_3(CO)_{12}]$ transforms photochemically into a transient ($\tau \approx 55$ ps) with a single CO bridge (Figure 1).[9] By contrast, two different bridging carbonyl ligands have recently been

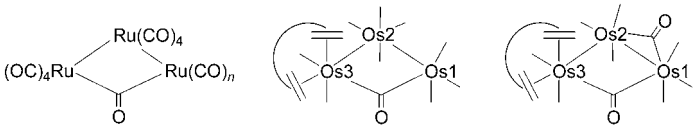

Figure 1. Proposed schematic structures of the open-core photoproducts $[Ru_3(CO)_{11}(\mu\text{-}CO)]$ ($n=3$),[14] $[Ru_3(CO)_{12}(\mu\text{-}CO)]$ ($n=4$)[15] (left), $[Os_3(CO)_9(\mu\text{-}CO)(1,3\text{-diene})]$ (middle) and $[Os_3(CO)_8(\mu\text{-}CO)_2(1,3\text{-diene})]$[11] (right).

identified by Bakker et al. by ns TRIR spectroscopy in a photoproduct of the substituted cluster $[Os_3(CO)_{10}(s\text{-}cis\text{-}cyclohexa\text{-}1,3\text{-}diene)]$.[11] This cluster represents osmium–diene compounds that may serve as activated precursors for various synthetic applications.[12,13] In analogy to the reactive photoisomer of $[Ru_3(CO)_{12}]$, the nonradical photoproduct of $[Os_3(CO)_{10}(s\text{-}cis\text{-}1,3\text{-}cyclohexadiene)]$ was proposed to have one Os–Os(1,3-diene) bond split and the two remote osmium centres connected by a bridging carbonyl group (Figure 1). The resulting electron deficiency at Os1 was then considered partly compensated by donation from another carbonyl group bridging over the Os1–Os2 bond. The 1,3-diene ligand was assumed to retain its *s-cis* coordination at Os3. This tentative structure of the ns transient was found to correspond well to the fragmentation into $\{Os_2(CO)_6(\mu\text{-}CO)(L)_2\}$ and $\{Os(CO)_3(1,3\text{-diene})\}$ in the presence of L = CO, olefin.

In this work we present the results of a combined ps TA and TRIR study of the photoreactivity of $[Os_3(CO)_{10}(s\text{-}cis\text{-}cyclohexa\text{-}1,3\text{-}diene)]$ (**1**). The ps TA spectra were recorded in order to determine the decay kinetics of the excited state and its absorption features. The ps TRIR study was aimed towards gaining more information about cluster **1** in its reactive excited state and towards monitoring, with a suitable time resolution, the formation of the two different CO bridges in the nonfragmented ultimate photoproduct. Importantly, density functional theory (DFT and TD-DFT) calculations were performed 1) on the geometry-optimised clusters $[Os_3(CO)_{10}(buta\text{-}1,3\text{-}diene)]$ (**2′** and **2″**) in order to support the interpretation of the experimentally acquired time-

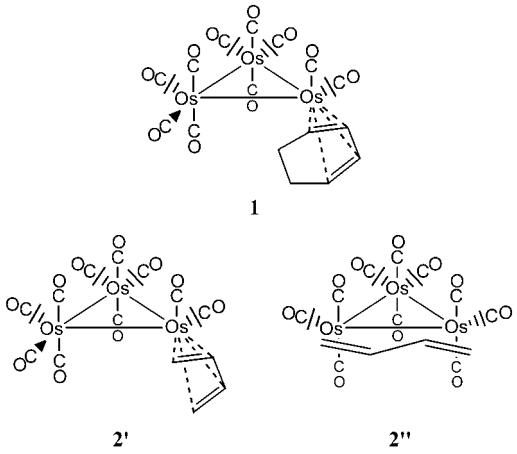

resolved spectroscopic data, and 2) on the short-lived photochemical transients to obtain information about their possible geometries and for better understanding of the photoreaction pathway. The latter goal is unprecedented in cluster photochemistry. In particular, we wondered whether the 1,3-diene ligand could also be involved in the stabilisation of the transient geometries.

Results and Discussion

DFT calculations on clusters $[Os_3(CO)_{10}(buta\text{-}1,3\text{-}diene)]$: Density functional theory (DFT) calculations were performed in order to understand the bonding properties of the $[Os_3(CO)_{10}(s\text{-}cis\text{-}buta\text{-}1,3\text{-}diene)]$ (**2′**) cluster and to assign its low-lying electronic transitions. This cluster provides a good model for the cyclohexa-1,3-diene cluster (**1**) used in the experiments. The crystal structures of $[Os_3(CO)_{10}(s\text{-}cis\text{-}buta\text{-}1,3\text{-}diene)]$ (**2′**) and its isomer $[Os_3(CO)_{10}(s\text{-}trans\text{-}buta\text{-}1,3\text{-}diene)]$ (**2″**) have been reported.[16,17] In **2′**, the buta-1,3-diene ligand is coordinated to a single osmium centre in a chelating fashion and a *cis* arrangement, with one C=C bond equatorial and the other in an axial position (*s-cis*). Isomer **2″**, with approximate C_2 symmetry, has the *trans*-buta-1,3-diene ligand bridging over an Os–Os bond, with both C=C bonds in equatorial positions (*s-trans*). The optimised structures of the two isomers **2′** and **2″** are depicted in Figure 2.

Isomer **2″**, with the 1,3-diene ligand coordinated in the *trans* fashion and bridging, is slightly more stable (10 kJ mol^{-1}). The small energy difference does not prevent $[Os_3(CO)_{10}(s\text{-}cis\text{-}buta\text{-}1,3\text{-}diene)]$ (**2′**) from being obtained in high yields both from $[H_2Os_3(CO)_{10}]$[16] and from $[Os_3(CO)_{10}(MeCN)_2]$,[11] the latter cluster even being pre-activated for the *s-trans* geometry, due to the coordination of the MeCN ligands at different osmium centres.[18]

The optimised geometries of isomers **2′** and **2″** are in good agreement with the experimentally determined structures (Tables SI1 and SI2, respectively, in the Supporting Information). The reproduction of the Os–Os distances in particular has proven difficult in the past,[12,19] but with better basis sets, as used in this work, the agreement is better. For **2′**, the three experimentally ascertained Os–Os distances are

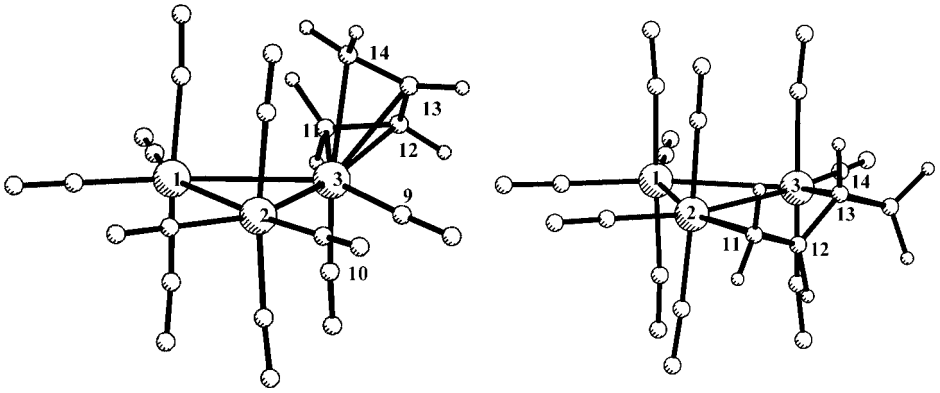

Figure 2. Optimised geometries of the isomeric clusters **2′** (= *s-cis*; left) and **2″** (= *s-trans*; right).The relative energies are 10 and 0 kJ mol^{-1} for **2′** and **2″**, respectively.

2.863(3), 2.861(3) and 2.884(3) Å, very similar to the calculated values of 2.943, 2.921 and 2.941 Å, respectively. For cluster **2″**, the two sets of distances are 2.858(3), 2.856(3) and 2.932(3) Å (experimental) and 2.934, 2.931 and 2.987 Å (calculated), the longest distance corresponding to the Os–Os bond spanned by the bridging ligand. As cluster **1** was used in the ps TRIR photochemical studies, the following discussion refers only to the corresponding *s-cis* isomer of $[Os_3(CO)_{10}$(buta-1,3-diene)] (**2′**).

The composition of the molecular orbitals of cluster **2′** corresponds to the data given in Table 1, with the HOMO (H) and LUMO (L) indicated in bold. Three-dimensional representations of the three highest occupied molecular orbitals (HOMO, HOMO−1 and HOMO−2) and of the lowest unoccupied molecular orbital (LUMO) are depicted in Figure 3. The LUMO of **2′** has a predominantly axial π*(CO) character, together with small osmium–osmium antibonding contributions. The HOMO has significant contributions from all three metal centres and the equatorial carbonyl groups; it is mainly σ-bonding between the Os1 and Os3(1,3-diene) centres, and can therefore be described as a σ(Os1–Os3) bonding orbital. By contrast, the HOMO−1 is mainly localised on Os3, the diene ligand and one axial carbonyl group, corresponding to the back donation from Os3 to these two ligands, and can be assigned as a π(C=C–Os3–C(10)O) bonding orbital. All three metal centres participate in the HOMO−2, that is, σ-bonding between Os1 and Os2 and σ-bonding between Os3 and the equatorial C=C bond of the 1,3-diene ligand. The HOMO−3 has a character similar to that of the HOMO, with significant contributions from all three metal centres and the carbonyl groups. From the natures of the frontier orbitals, the predominant character of the HOMO–LUMO transition can be described as σ(Os1–Os3)-to-π*(CO). The excitation energies and the oscillator strengths of the singlet–singlet low-lying electronic transitions of **2′** were calculated by TD-DFT methods and are presented in Table 2.

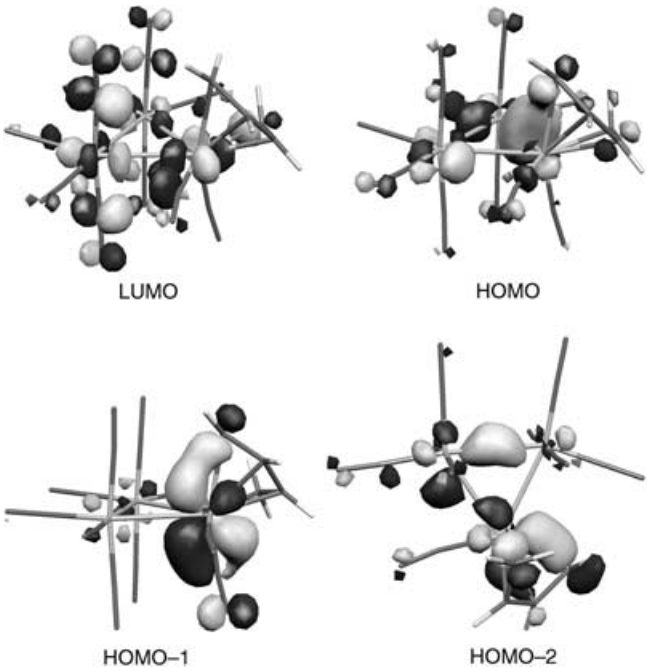

Figure 3. Three-dimensional plots of the frontier orbitals of geometry-optimised $[Os_3(CO)_{10}$(*s-cis*-buta-1,3-diene)] (**2′**).

Table 1. Compositions [%] and energies of selected frontier molecular orbitals (MOs) of the geometry-optimised cluster $[Os_3(CO)_{10}$(*s-cis*-buta-1,3-diene)], **2′** (L = LUMO, H = HOMO).

MO		*E* [eV]	Os1[a]	Os2[a]	Os3[a]	diene	CO
110 a	L+3	−2.52	2.2	1.2	5.7	6.5	84.6
109 a	L+2	−2.69	5.5	4.3	1.5	0.6	85.4
108 a	L+1	−2.96	2.2	2.9	4.4	3.7	86.0
107 a	**L**	**−3.39**	**7.4**	**9.6**	**10.4**	**6.3**	**61.0**
106 a	**H**	**−5.96**	**25.7**	**12.0**	**12.2**	**12.5**	**30.1**
105 a	H−1	−6.20	4.3	3.6	57.3	9.6	18.9
104 a	H−2	−6.32	8.5	17.9	24.3	22.4	19.8
103 a	H−3	−6.57	24.2	14.6	15.9	6.6	34.2

[a] See Figure 2.

Electronic absorption spectra of $[Os_3(CO)_{10}$(*s-cis*-buta-1,3-diene)] (2′): The electronic absorption spectrum of cluster **1** in hexane shows a non-solvatochromic lowest energy absorption band around 400 nm, close to a more intense band at 331 nm. Similar absorption bands are also present in the spectra of $[Os_3(CO)_{10}$(*s-cis*-buta-1,3-diene)] (**2′**) (Figure 4). The positions of the absorption maxima of the two low-lying bands of cluster **2′** are in good agreement with the calculated TD-DFT values for its optimised geometry (Table 2).

Table 2. TD-DFT calculated low-energy excitation energies (E) and oscillator strengths (O.S.) for the geometry-optimised cluster $[Os_3(CO)_{10}(s\text{-}cis\text{-buta-1,3-diene})]$, **2′**.

Transition	Composition	E [eV]	λ [nm]	λ_{max}[a] [nm]	O.S. ($\times 10^3$)
1	69% (H→L), 15% (H−1→L)	2.82	440		18
2	84% (H−1→L), 11% (H→L)	2.88	431		4.3
3	89% (H→L+1)	3.07	404		7.6
4	63% (H−2→L), 18% (H−3→L), 7% (H→L)	3.14	395	400[b]	29
5	62% (H→L+2), 21% (H−3→L), 10% (H−2→L)	3.31	375		10
6	42% (H−3→L), 25% (H→L+2), 12% (H−2→L+1)	3.39	366	331[c]	16
7	46% (H→L+3), 31% (H−3→L+1), 6% (H−2→L+1)	3.59	346		12

[a] Observed absorption maxima for $[Os_3(CO)_{10}(s\text{-}cis\text{-buta-1,3-diene})]$ (**2′**) in hexane at 293 K.[11] [b] Asymmetric band with shallow resolved maximum (ca. 380 nm) and a shoulder around 410 nm. It probably comprises the calculated transitions 1–4. [c] This absorption band probably comprises the calculated transitions 5–7.

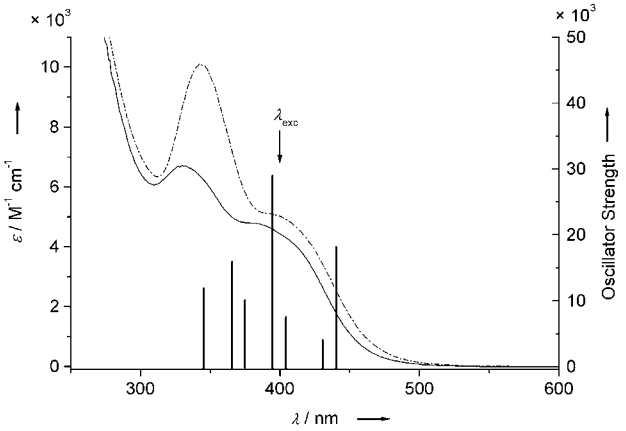

Figure 4. UV/Vis spectra of clusters $[Os_3(CO)_{10}(s\text{-}cis\text{-cyclohexa-1,3-diene})]$ (**1**) (–•–•) and $[Os_3(CO)_{10}(s\text{-}cis\text{-buta-1,3-diene})]$ (**2′**) (——) in hexane at 293 K. Major electronic transitions of cluster **2′** as calculated with the ADF program (see Table 2).

As the absorption features in the visible region are generally broad and poorly resolved, the first four electronic transitions (440–395 nm, Table 2) most probably contribute to the lowest energy band. These allowed transitions are directed to the LUMO and LUMO+1 orbitals, which have predominant cluster-core–π*(CO) characters. At a higher energy, a second group of fairly intense transitions is found (close-lying transitions 5–7, Table 2). Like the first group, these transitions are mainly directed to π*(CO) orbitals, while the parent occupied orbitals (HOMO, HOMO−2 and HOMO−3) are bonding with respect to specific metal–metal bonds within the cluster core. The intense 331 nm band in the UV/Vis spectrum of $[Os_3(CO)_{10}(s\text{-}cis\text{-buta-1,3-diene})]$ (**2′**) therefore also has a σ(core)π*(CO) character.

The TD-DFT results thus reveal that the electronic transitions of $[Os_3(CO)_{10}(s\text{-}cis\text{-buta-1,3-diene})]$ (**2′**) in the visible region have a predominant σ(core)π*(CO) character. The calculated excitation energies and oscillator strengths compare reasonably well with the experimentally obtained data for **2′** recorded in hexane. Excitation into the σ(core)-to-π*(CO) transitions does not result in large perturbations of the cluster bonds in systems like the nonsubstituted precursor $[Os_3(CO)_{12}]$, in which selective irradiation into its lowest-energy σ(core)π*(CO) absorption band does not trigger any significant photoreactivity.[20] By contrast, visible irradiation of cluster **1** partly results in its fragmentation into mono- and dinuclear complexes.[11] The difference in the photoreactivity of cluster **1** in relation to symmetric $[Os_3(CO)_{12}]$ presumably lies in a more pronounced weakening of Os−Os bonds on excitation, caused by the donor ability of the 1,3-diene ligand. This situation should facilitate the cleavage of the Os1−Os3 and Os2−Os3 bonds, especially in the presence of a coordinating Lewis base. It remains undecided, however, whether the initial bond-cleavage reaction, as discussed in more detail below, takes place straightforwardly from a reactive σπ* state,[21] or through an interaction of the σπ* state with a rapidly decaying dissociative state of a σσ* character. A similar avoided crossing along the reaction coordinate, which transforms the σπ* state into a dissociative state, occurs in the clusters $[Os_3(CO)_{10}(\alpha\text{-diimine})]$.[22]

Picosecond time-resolved spectroscopy of $[Os_3(CO)_{10}(s\text{-}cis\text{-1,3-cyclohexadiene})]$ (1): In order to investigate the primary events following the photoexcitation of cluster **1**, picosecond transient absorption (ps TA) spectra were recorded in hexane and CH_2Cl_2. The ps TA spectra were obtained by excitation at 430 nm, and spectral changes were monitored in the 450–650 nm wavelength region. Kinetic profiles were probed at 500 nm in 250 fs intervals up to 15 ps. The ps TA spectra of **1** in CH_2Cl_2, measured 1–10 ps after the 130 fs laser pulse, are depicted in Figure 5, and the corresponding kinetic profile is shown in Figure 6.

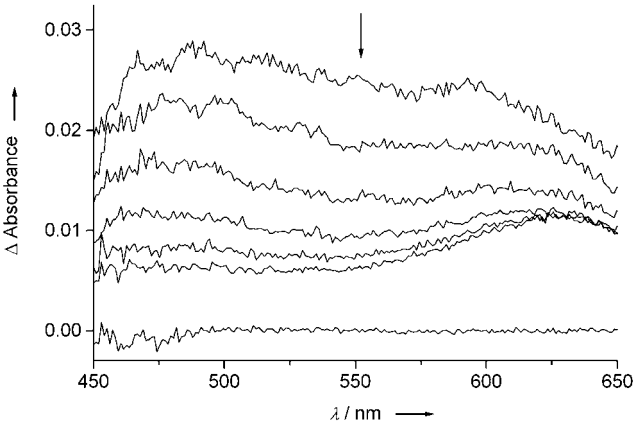

Figure 5. Transient difference absorption spectra of cluster **1** in CH_2Cl_2, measured at time delays of −1 (baseline), 1, 2, 3, 5, 8 and 10 ps, respectively, after FWHM excitation (430 nm, 130 fs).

The ps TA spectrum of cluster **1** in CH_2Cl_2 recorded at $t_d = 1$ ps (Figure 5) shows two broad, overlapping transient absorption bands with maxima around 505 nm and 595 nm. Within 10 ps, the lowest-energy band becomes considerably

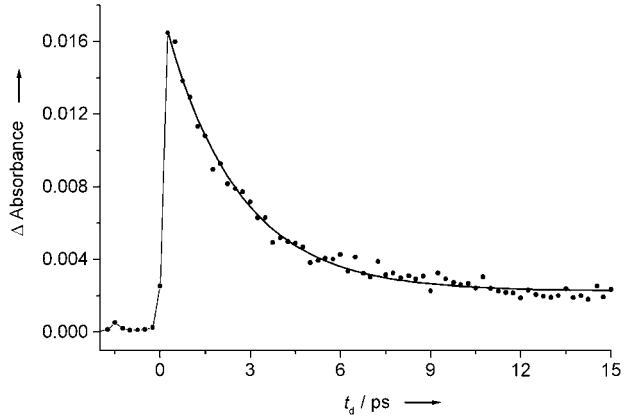

Figure 6. Kinetic profile of the difference absorption of cluster **1** in CH_2Cl_2, probed at 500 nm after FWHM excitation (430 nm, 130 fs).

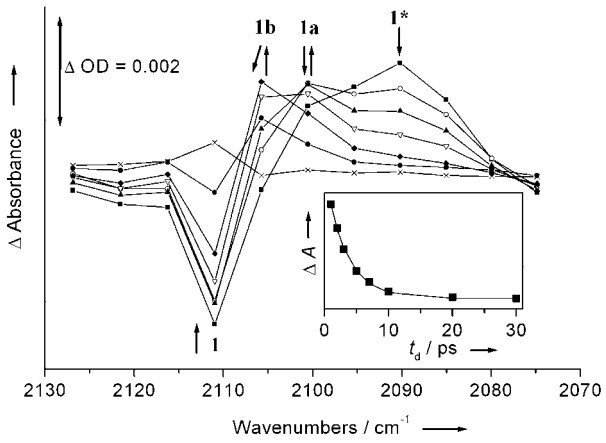

Figure 7. TRIR difference spectra of cluster **1** in heptane between 2130–2070 cm^{-1}: (■) 1 ps, (○) 2 ps, (▲) 3 ps, (▽) 5 ps, (◆) 10 ps, (●) 40 ps and (×) 500 ps after 400 nm (ca. 150 fs FWHM, 5 μJ per pulse) excitation. Inset: kinetic trace representing the decay of the 2090 cm^{-1} band.

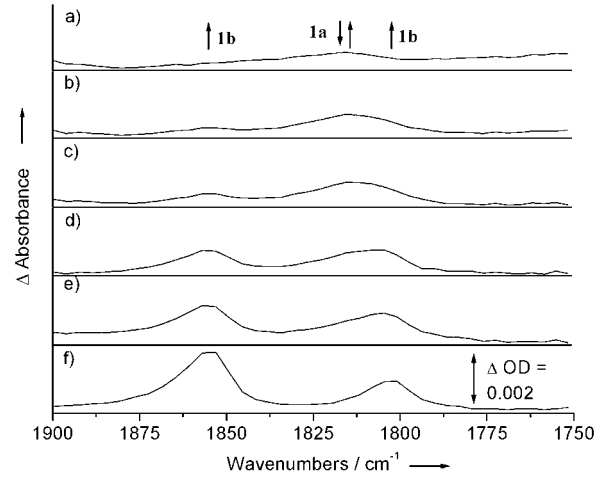

Figure 8. TRIR difference spectra of cluster **1** in heptane between 1900–1750 cm^{-1}: a) 1.5 ps, b) 2.5 ps, c) 3 ps, d) 5 ps, e) 7 ps and f) 20 ps after 400 nm (ca. 150 fs FWHM, 5 μJ per pulse) excitation.

red-shifted and transforms into a broad, well-resolved absorption band with a distinct maximum at 630 nm. On the same timescale, the band at 505 nm initially shows a small blue shift, to 480 nm at $t_d = 4$ ps. After this time delay no distinct maximum can any longer be observed between 450 and 550 nm and only a broad unresolved absorption remains. The kinetic profile of **1** probed at 500 nm is clearly monoexponential in both hexane and CH_2Cl_2 and provides an excited state lifetime of 2.5 ± 0.1 ps (Figure 6). The transient absorption at $t_d = 10$ ps is very similar to that observed by Bakker et al. in the ns TA spectra of this cluster and assigned to the photoproduct $[Os_3(CO)_8(\mu\text{-}CO)_2(L)]$ (L = cyclohexa-1,3-diene).[11] In order to verify that the absorptions in the ps and nanosecond time domains refer to the same species, we also measured the TA spectra at 300, 600 and 900 ps after the laser pulse. These spectra do not differ from those measured at 10 ps or at 10 ns. From this observation we conclude that the double CO-bridged photoproduct previously observed on the nanosecond timescale is already present in the picosecond time domain.

Another important aim of this work was to find out whether the different bridging carbonyl ligands in the photoproduct $[Os_3(CO)_8(\mu\text{-}CO)_2(\text{cyclohexa-1,3-diene})]$ are formed in a stepwise fashion or directly from the excited state in a concerted process. For this purpose, ps TRIR spectra of cluster **1** were recorded in heptane after 400 nm excitation at several pump–probe delays between 0 and 500 ps. Representative difference IR spectra in the 2130–2070 cm^{-1} and 1900–1750 cm^{-1} regions are shown in Figures 7 and 8, respectively. The extensive overlap between the bleached ν(CO) bands of the complex in the ground state and the excited-state absorptions largely precludes assignment of the excited-state CO-stretching modes. In fact, only the clearly separated highest frequency band at 2111 cm^{-1} could be used to monitor the population of the excited state and the subsequent formation of photoproducts. After irradiation into the lowest energy absorption band of **1** in heptane, the ps TRIR spectra at early time delays (< 3 ps) display instantaneous bleaching of the parent ν(CO) bands (negative signals), together with broad transient absorption bands due to the excited state of **1**. The highest frequency ground-state band at 2111 cm^{-1} becomes shifted to smaller wavenumbers in the excited state (2090 cm^{-1}, Figure 7). This behaviour is in line with the population of an excited state having a predominant $\sigma\pi^*$ character, and results from a decrease in the C–O bond order due to the population of anti-bonding π^*(CO) orbitals. If the lowest excited state were localised at the metal core with mainly a $\sigma\sigma^*$ character, a decrease in the π back-bonding to the carbonyl ligands would be expected, resulting in a shift of the ν(CO) bands in the opposite direction. At $t_d = 1$ ps, the transient ν(CO) band at 2090 cm^{-1} exhibits a high-frequency shoulder around 2100 cm^{-1} that develops into a distinct band at the expense of the band at 2090 cm^{-1}, reaching its maximum intensity at about 2.5 ps. At longer time delays (up to 10 ps), the latter band also decays and a new ν(CO) band appears at 2106 cm^{-1}, and further shifts to 2111 cm^{-1} at $t_d = 500$ ps. The remaining difference spectrum at $t_d = 500$ ps closely resembles the reported difference IR spectrum of cluster **1** on the nanosecond timescale.[11]

In order to monitor the CO-bridge formation, we focused on the IR spectral changes in the 1900–1750 cm^{-1} region. After excitation of cluster **1** at 400 nm, the ps TRIR spectra at early time delays (< 5 ps) show the appearance of a broad ν(μ-CO) band around 1815 cm^{-1}, reaching its maximum intensity after approximately 3 ps (Figure 8). This point having been reached, a shoulder at 1801 cm^{-1} and a new band at 1857 cm^{-1} further develop at the expense of the 1815 cm^{-1} band. At $t_d = 20$ ps, the initial ν(μ-CO) band has completely disappeared and only the two new ν(μ-CO) bands at 1801 and 1857 cm^{-1} are present, their intensity not changing up to 500 ps. Importantly, these ν(μ-CO) bands closely resemble those observed on the nanosecond timescale.[11]

The ps TRIR spectra of cluster **1** in the 1900–1750 cm^{-1} region reveal that the two different CO-bridges in the photoproduct $[Os_3(CO)_8(\mu\text{-}CO)_2(\text{cyclohexa-1,3-diene})]$ (**1b**) form stepwise. Initially, primary photoproduct **1a** is rising, showing only a single ν(μ-CO) band at 1815 cm^{-1}. The observation of this band already at 1.5 ps after the laser pulse implies that population of the reactive σπ* excited state (vide supra) occurs on the sub-picosecond timescale. The ps TRIR spectra do not reveal whether at $\lambda_{exc} = 400$ nm the π*(CO) orbitals are populated from a molecular orbital with predominant σ(Os1–Os3) (HOMO) or σ(Os1–Os2) (HOMO–2) character (Table 2). From the nature of the fragmentation products formed upon continuous-wave irradiation of cluster **1**,[11] the Os1–Os2 bond connecting the two Os centres in the dinuclear photoproducts $[Os_2(CO)_6(\mu\text{-}CO)(L)_2]$ (L = CO, ethene) should remain intact. As this reasoning does not agree with the depopulation of the HOMO–2 (Figure 3), it is proposed that the reactive σπ* excited state should have σ(Os1–Os3)π*(CO) (HOMO–LUMO) character. On the other hand, the depopulation of the HOMO–2 (Figure 3) should also weaken the bond between Os3 and the equatorial C=C bond of the 1,3-diene ligand (vide supra), contributing to electron deficiency at the Os3 centre. The DFT study of the primary photochemical transient (vide infra) shows us that this situation can also be of importance for triggering the photoreaction. The ps TRIR study thus indicates that the first carbonyl bridge forms in order to compensate for electron deficiency at the Os3 centre. However, it does not allow us to decide whether the carbonyl ligand is spanned over a cleaved or intact Os–Os bond, for the 1,3-diene ligand may also be forming a bridge (vide infra).

In a second step, transient **1a** rapidly transforms, within a few picoseconds, into secondary photoproduct **1b** with two different CO bridges. This process involves the movement of another terminal CO ligand to a bridging position in order to compensate further for electron deficiency in the cluster core caused by the primary photochemical event. Also in this case, the structural information from the ps TRIR spectra is limited and a theoretical study of **1b** (vide infra) was needed in order to distinguish between several possibilities. In the primary photoproduct of the symmetric cluster $[Ru_3(CO)_{12}]$[14] (Figure 1), the electron density is equally distributed over the CO-bridged Ru centres. The movement of a second carbonyl to a bridging position is therefore redundant in this case. The consecutive formation of the different carbonyl bridges upon the excitation of cluster **1** is also reflected in the IR spectral changes in the terminal ν(CO) region (Figure 7). The transient ν(CO) band at 2100 cm^{-1} grows in on the same timescale as the ν(μ-CO) band at 1815 cm^{-1} and can therefore be ascribed to transient **1a**. As this band develops at the expense of the 2090 cm^{-1} band, the latter can be assigned to the σπ* excited state of **1**. Finally, the ν(CO) band at 2106 cm^{-1}, which in turn grows at the expense of the 2100 cm^{-1} band, reaches its maximum intensity at the same time delay as the ν(μ-CO) bands at 1857 and 1801 cm^{-1} and is therefore attributable to **1b**. As the ν(μ-CO) bands at 1801 and 1857 cm^{-1} do not change in intensity or position after $t_d = 20$ ps, the shift of the 2106 cm^{-1} band to 2111 cm^{-1} at longer time delays ($t_d >$ 50 ps) is not ascribed to the formation of a new thermal product, but most probably reflects a structural rearrangement within **1b**. In general, the shift of the highest frequency ν(CO) band of cluster **1** in the excited state to larger wavenumbers upon formation of **1a** and **1b** reflects the decreased π back-bonding towards the terminal CO ligands, in line with the consecutive formation of the two more strongly π-accepting CO bridges.

In order to describe the observed kinetics in a qualitative way, the formation of photoproduct **1b** is represented by two consecutive irreversible first-order reactions (Scheme 1). After excitation of **1**, quantitative formation of

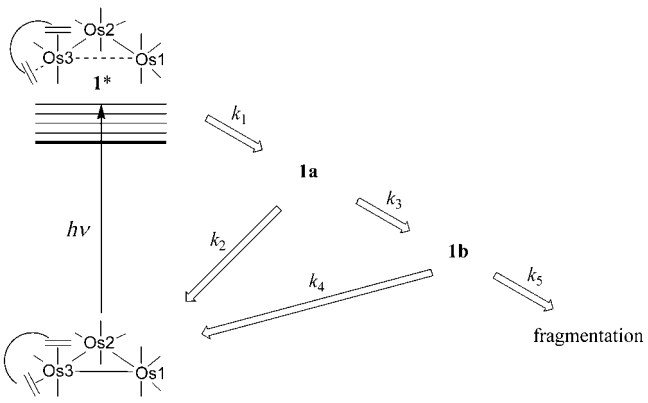

Scheme 1. Schematic representation of the primary events taking place after photoexcitation of cluster **1**. The structures of transient **1a** and photoproduct **1b** are discussed in the main text and shown in Figure 9.

the transient **1a** from the excited state **1*** is assumed (rate constant k_1). This is inferred from the negligible change in intensity of the highest frequency bleach of **1** at 2111 cm^{-1} at t_d between 2 and 3 ps, whereas the ν(CO) band at 2090 cm^{-1} due to the excited state (**1***) significantly decreases. In a second step, primary photoproduct **1a** can either regenerate the parent cluster (rate constant k_2) or transform into **1b** with rate constant k_3. Finally, photoproduct **1b** mainly regenerates the parent cluster (ca. 70%, rate constant k_4), while a small part of the molecules fragments into mono- and dinuclear products (ca. 30%, k_5).[11] As the last two processes only take place in the nanosecond time domain ($\tau_{1b} = 94$ ns in hexane),[11] k_4 and k_5 do not influence

the kinetics on the early picosecond timescale (i.e., k_1 and k_3). According to the mechanism depicted in Scheme 1, the reactive σπ* excited state **1*** decays mono-exponentially with a lifetime $1/k_1$. Although both vibrational cooling processes and the decay of the excited state take place on similar timescales, the excited-state lifetime ($\tau_{\mathbf{1}^*} = 3.3 \pm 0.1$ ps) was estimated by plotting the integrated intensity of the 2090 cm^{-1} band against time (Figure 7, inset). In accordance with the development of the 1815 cm^{-1} band, this implies that photoexcitation of cluster **1** results in rapid cleavage of an Os–Os(diene) bond, accompanied by the formation of a single CO bridge in transient **1a** ($k_1 = 3 \times 10^{11}$ s^{-1}). In the proposed mechanism the concentration of **1a** over time is described by the kinetics of a consecutive process, which unfortunately cannot be solved from the available experimental data. However, as **1a** is clearly observable by means of the ν(CO) bands at 1815 and 2100 cm^{-1}, its conversion to **1b** together with the decay to the ground state ($k_2 + k_3$) must be slower than its formation from the excited state (k_1). Moreover, as the absorption molar coefficients of the ν(μ-CO) bands of **1a** and **1b** are assumed to be similar, the fairly high intensity of the ν(CO) bands at 1801 and 1857 cm^{-1} (**1b**) also indicates that regeneration of the parent cluster from transient **1a** is either a process of minor importance ($k_2 < k_3$) or does not take place at all. Formation of photoproduct **1b** is therefore concluded to be the rate-determining step.

The excited state lifetime of 3.3 ps, derived from the TRIR experiments, closely resembles the value of 2.5 ps obtained from the TA measurements. Consistently with the TRIR experiments, the UV/Vis spectral changes within the first 10 ps after excitation (Figure 5) represent both the formation of **1a** from the σπ* excited state and its conversion into **1b**. As the 500 nm kinetic profile of cluster **1** in CH_2Cl_2 (Figure 6) is clearly mono-exponential and the ν(μ-CO) bands attributed to **1b** only reach their maximum intensity after about 20 ps (Figure 8), the initial 2.5 ps TA process mainly corresponds to the decay of the excited state and concomitant formation of **1a**. As no kinetic change is observed at 500 nm upon subsequent formation of **1b**, both photoproducts **1a** and **1b** are assumed to absorb similarly around this wavelength.

DFT study of models of transient 1a and photoproduct 1b: DFT calculations were performed in order to provide more insight into the possible structures of transient **1a** and photoproduct **1b**, by use of the geometry-optimised buta-1,3-diene cluster **2′** (Table SI1 in the Supporting Information). It is well known that carbonyl triosmium clusters do not favour the presence of bridging carbonyl groups unless a very strong σ-donor ligand is present, which is not the case.[3] Therefore, in the attempts to obtain structures with bridging carbonyl groups, some constraints had to be kept in the initial steps of the optimisation procedure, forcing one or more carbonyl ligands to remain bridging (see Experimental Section for more details). Two structures could be found, both at significantly higher energies than parent cluster **2′** (see Figure 9).

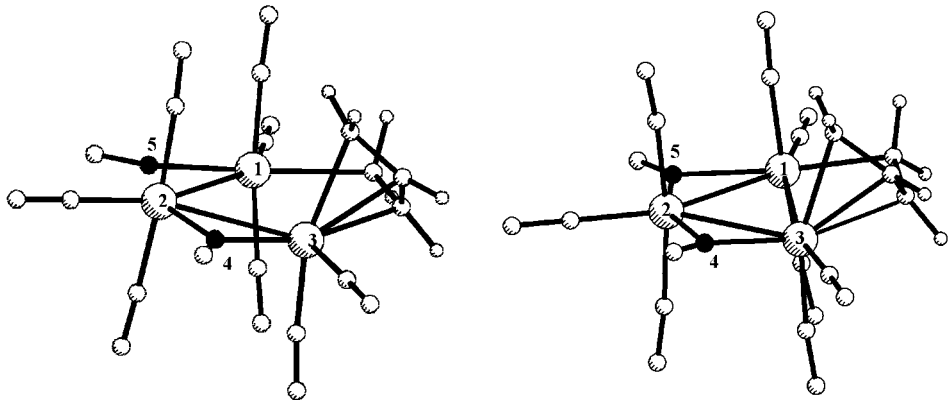

Figure 9. Calculated (ADF program) geometries of transient **2a** (left) and photoproduct **2b** (right). The energies, relative to those of geometry-optimised cluster **2′** (Figure 2), are 101 and 50 kJ mol^{-1} for **2a** and **2b**, respectively. The dark circles represent the carbon atoms of the bridging or semi-bridging carbonyl groups.

Most notably, in both calculated structures the 1,3-diene coordination has changed from purely chelating to bridging, as one carbon atom already binds at the adjacent Os1 atom. In **2a**, there is one bridging CO group (Os2,3–C4 distances: 1.894, 2.047 Å) and another one, which can be called semi-bridging, being severely distorted (Os1,2–C5 distances 2.007, 2.494 Å) toward making a bridge. On the other hand, there are two bridging carbonyl groups in **2b** (Os1,2–C5 distances 2.195, 2.085 Å; Os2,3–C4 distances 2.250, 2.032 Å). The Os–Os distances (Table 3) are misleading and cannot be used directly to compare bond strengths. As has been shown before,[19] the formation of a bridging carbonyl results in an increased metal–metal repulsion, which should lead to a longer intermetallic distance. However, the small bite of the carbonyl ligand prevents this relaxation from occurring, and the distance remains short. Therefore, Wiberg and Mayer indices, which can be used as indicators of bond strengths, were also calculated, and are shown in Table 3. The Wiberg indices[23] are the result of a natural population analysis[24] by Gaussian 98, while Mayer indices[25] can be directly calculated from the ADF data by using the MAYER program.[26] For comparison, the same values are given in Table 3 for parent cluster **2′**.

Several conclusions can be drawn from the values in Table 3. In the structure **2a**, the Os2–Os3 bond keeps the same distance (2.940/2.941 Å), but both Wiberg and Mayer indices show that the bond is weaker (0.118 and 0.295, compared to 0.220 and 0.424, respectively, in geometry-optimised **2′**). A carbonyl group is bridging over these two osmium atoms. The Os1–Os2 and Os1–Os3 bonds become slightly longer, but much weaker, as reflected in both indices. From **2a** to **2b**, the Os1–Os2 bond shortens the most.

Table 3. Calculated Os–Os and Os–$C(O)_{bridge}$ bond lengths [Å], and Wiberg and Mayer indices in photoproducts **2a** and **2b**, as well as in geometry-optimised parent cluster **2′**.

Bond[a]	**2a** Length	**2a** Wiberg indices	**2a** Mayer indices	**2b** Length	**2b** Wiberg indices	**2b** Mayer indices	**2′** Length	**2′** Wiberg indices	**2′** Mayer indices
Os1–Os2	3.029	0.110	0.326	2.869	0.146	0.374	2.921	0.197	0.493
Os1–Os3	3.166	0.119	0.325	3.125	0.139	0.370	2.943	0.214	0.439
Os2–Os3	2.940	0.118	0.295	2.958	0.118	0.293	2.941	0.220	0.424
Os1–C5	2.007	0.707	0.862	2.195	0.475	0.582	–	–	–
Os2–C5	2.494	0.199	0.329	2.085	0.547	0.708	–	–	–
Os2–C4	1.894	0.727	0.888	2.250	0.362	0.529	–	–	–
Os3–C4	2.047	0.592	0.673	2.032	0.697	0.789	–	–	–

[a] See Figure 9.

The Wiberg indices and Mayer indices drop from 0.197 and 0.493 for **2′** to 0.146 and 0.374 in **2b**, respectively. For the other two Os–Os bonds, the increase in length is accompanied by the expected decrease in strength. These results demonstrate that bond length cannot be used reliably to estimate bond strength in clusters containing bridging carbonyl groups. In general, we can conclude that all Os–Os bonds weaken in the transient and in the photoproduct.

To check the agreement between the theoretical and experimentally determined structures of the photoproduct, IR CO-stretching wavenumbers of the bridging carbonyl groups in **2b** were calculated by the DFT method to be 1864 and 1832 cm^{-1}. In view of the limitations, the calculated values compare fairly well with those of 1857 and 1801 cm^{-1} measured for **1b** (vide supra). This result demonstrates the difference between the CO bridges. Even though they each span an Os–Os bond, the weakened Os–Os bonds are not equivalent. In previous work,[11] one of the carbonyl groups was assumed to bridge the open Os1–Os3 bond instead of the 1,3-diene ligand, in analogy to the transients $[Ru_3(CO)_n(\mu\text{-}CO)]$ ($n = 11, 12$).[14,15] No similar attempt could be made for **2a**, since the low stability of the product forced a constrained geometry optimisation and prevented a meaningful frequency calculation.

Remarks on the photoreactivity of clusters 1 and 2′: Apart from the ps–ns TA and TRIR data, and the assignment of the products of the photofragmentation,[11] the TD-DFT study of the parent clusters and the transients/photoproducts provides an important basis for a more detailed analysis of the initial steps in the photoreaction mechanism of clusters **1** and **2′** (Scheme 1). Importantly, the theoretical results are in favour of the cleavage of an Os–Os(1,3-diene) bond from the initially populated σπ* excited state. According to the strong involvement of the HOMO in the lowest σπ* excited state (Table 2), the cleavage concerns the Os1–Os3 bond. As a response to this dissociation step and the resulting electron deficiency at the Os1 centre, the former Os1–Os3 bond becomes bridged by the 1,3-diene ligand, using one of its C=C π systems, bound in the parent cluster exclusively to the Os3 atom, in the equatorial position. As mentioned above, the involvement of the HOMO−2 in the low-energy photoexcitation (Table 2) may also facilitate this development. The preferential bridging coordination of the 1,3-diene (see also Figure 2), not considered in the previous tentative mechanism,[11] may reflect its higher donor ability and larger bite angle in relation to those of CO. The first CO bridge over the Os2–Os3 bond is most probably formed in a concerted way in the sub-picosecond time domain, to compensate for some electronic deficiency at the Os3 centre. In the calculated coordinatively unsaturated transient **2a** (corresponding to **1a** in Scheme 1), the Os1–Os3 bond is drawn open (Figure 9), in agreement with the 18-electron count rule at the Os1 centre, even though the other two Os–Os bonds are also significantly weaker than in **2′**. The Os1–Os2 bond is stabilised by the formation of the second carbonyl bridge in **2b** (representing **1b** in Scheme 1) in the picosecond time domain and becomes the strongest metal–metal bond in the photoproduct. This explains why this particular bond does not cleave upon coordination of Lewis bases (CO, olefins) at this stage.[11] According to Table 3, it is likely that the Os1–Os3 bond is restored in the photoproduct and that **2b** is a fully bridged coordination isomer of parent cluster **2′**, converting in the nanosecond time domain back to the thermodynamic structure with stronger Os–Os bonds.

Conclusion

Picosecond TRIR spectroscopy has proven to be a powerful tool for obtaining some structural information about cluster **1** in its lowest excited state and for monitoring the conversion into photoproducts. In contrast to the photoreactivity of non-substituted $[Ru_3(CO)_{12}]$,[9] the IR spectral changes observed for cluster **1** reveal stepwise formation of two CO bridges, resulting in the photoproduct $[Os_3(CO)_8(\mu\text{-}CO)_2$(cyclohexa-1,3-diene)] (**1b**). The formation of the second CO bridge in the latter cluster is favoured by increased electron density in the transient $[Os_3(CO)_9(\mu\text{-}CO)$(cyclohexa-1,3-diene)] (**1a**) caused by the bridging coordination of the 1,3-diene ligand.

Both the experimentally measured data and the TD-DFT results support the assignment of the low-lying electronic transitions of **1** as having a predominant σ(core)-to-π*(CO) character. The reactive lowest σπ* excited state, most probably populated from the higher lying, optically accessible σ(Os1–Os2)π* state, is ascribed a σ(Os1–Os3)π*(CO) character. This assignment is supported by the structure of the transient species obtained by DFT calculations. Indeed, in

the calculated buta-1,3-diene transient **2a**, the Os1−Os3 bond is cleaved and bridged in the equatorial plane by the 1,3-diene ligand. In accordance with the ps TRIR spectra, a carbonyl bridge is also present, as well as a distorted carbonyl group. The latter will easily transform into a second bridge when forming the photoproduct. The Os1−Os2 bond, spanned by a bridging carbonyl group, is strengthened when **2a** converts into **2b**, preventing its cleavage during fragmentation reactions with Lewis bases. The experimental evidence for the bridging coordination of the 1,3-diene in the photogenerated species remains a challenge for the intended future studies.

Experimental Section

Materials and preparations: Solvents of analytical grade (Acros) were freshly distilled from sodium wire (hexane) or CaH_2 (acetonitrile (MeCN), dichloromethane) under an atmosphere of dry N_2. Cyclohexa-1,3-diene (Acros), dichloromethane, hexane and heptane (all Aldrich, spectroscopic grade) were used as received. Trimethylamine *N*-oxide, $Me_3NO{\cdot}2H_2O$ (Alfa), was dehydrated before use by vacuum sublimation. Silica 60 (70–230 mesh, Merck) for column chromatography was activated by heating under vacuum at 450 K overnight and stored under N_2.

Synthesis of $[Os_3(CO)_{10}$(*s-cis*-cyclohexa-1,3-diene)] (1): Cluster **1** was prepared under an inert atmosphere of dry N_2, by use of standard Schlenk techniques. We followed a synthetic procedure similar to that employed by Braga et al.,[27] with $[Os_3(CO)_{10}(MeCN)_2]$.[28]

Cyclohexa-1,3-diene (2.5 mL, 26 mmol) was added to a solution of $[Os_3(CO)_{10}(MeCN)_2]$ (500 mg, 0.54 mmol) in CH_2Cl_2 (70 mL). The reaction mixture was stirred for 2.5 h. After this period, the solvent was evaporated under vacuum. Purification of the crude product by column chromatography over silica with hexane/CH_2Cl_2 10:1 (v/v) as eluent gave cluster **1** as a yellow powder in 65% yield. ^{1}H NMR (300 MHz, $CDCl_3$, 293 K): $\delta = 5.58$ (dd, $^3J(H,H) = 5.3$ Hz, $^3J(H,H) = 3$ Hz, 2H; −CH=C*H*−C*H*=CH−), 3.76 (d, $^3J(H,H) = 7.2$ Hz, 2H; −C*H*=CH−CH=C*H*−), 1.87 ppm (br s, 4H; −CH_2−CH_2−); IR (hexane): $\tilde{\nu}$(CO) = 2111 (m), 2062 (s), 2032 (s), 2023 (vs), 2009 (s), 1991 (w), 1982 (m), 1974 (w), 1938 cm^{-1} (w); UV/Vis (hexane): λ_{max} (ε) = 244 (sh), 342 (10.1×10^3 mol^{-1} dm^3 cm^{-1}), 400 (sh) nm.

Spectroscopic measurements: Electronic absorption spectra were recorded on a Hewlett–Packard 8453 diode array spectrophotometer, FTIR spectra on a Bio-Rad FTS-7 spectrometer, and ^{1}H NMR spectra on a Bruker AMX 300 (300.13 MHz for ^{1}H) spectrometer.

Photochemistry: Picosecond transient absorption (ps TA) spectra and single-wavelength kinetic traces were recorded on the set-up installed at the University of Amsterdam.[22] Part of the 800 nm output of a Ti-sapphire regenerative amplifier (1 kHz, 130 fs, 1 mJ) was focussed into a H_2O flow-through cell (10 mm, Hellma) to generate white light. The residual part of the 800 nm fundamental was used to provide 430 nm (fourth harmonic of the 1500 OPA signal beam) excitation pulses with a general output of 5 μJ per pulse. After passing through the sample, the probe beam was coupled into a 400 μm optical fibre and detected with a CCD spectrometer (Ocean Optics, PC2000). Typically, two thousand excitation pulses were averaged to obtain the transient at a particular time delay. The picosecond time-resolved infrared (ps TRIR) spectra were recorded on the PIRATE set-up at the Central Laser Facility of the Rutherford Appleton Laboratory.[29] The laser system was based on a Ti-sapphire regenerative amplifier (Spectra Physics/Positive Light, Superspitfire), operating at 1 kHz repetition rate at about 800 nm, with an energy of 2–3 mJ per pulse (150 fs FWHM). Tuneable mid-IR outputs (150–200 cm^{-1} FWHM, 200 fs) were generated by frequency-down conversion of the signal and idler outputs of a white-light seeded, 800 nm pumped BBO OPA in an $AgGaS_2$ crystal. Second harmonic generation of the residual fundamental light (800 nm) provided 400 nm excitation pulses. The mid-IR beam generated by the first OPA was split into reference and probe beams with a 50% germanium beam-splitter. Below 1800 cm^{-1}, N_2-purged infrared beam paths were applied to reduce probe beam absorption by water vapour. The flow-through cell, consisting of two CaF_2 windows separated by 0.25–1 mm spacers, was allowed to make a rastering movement perpendicular to the probe beam in order to avoid local heating and sample decomposition by the laser beams. Two separate 64 element HgCdTe linear array detectors (MCT-13–64el (Infrared Associates Inc.) and MCT-64000 pre-amplifiers (Infrared Systems Development Corp.)) were used to detect the mid-IR reference and probe signals. TRIR spectra covering the whole CO-stretching region (2200–1700 cm^{-1}) were constructed from a precise overlap of three to four 150 cm^{-1} windows. Calibration of the spectra was established by comparison of the parent bleach positions with the peak positions of the corresponding ν(CO) bands in the regular FTIR spectra.

Computational details: Density functional theory (DFT) calculations[30] were carried out with the Amsterdam Density Functional (ADF-2002) program.[31] Vosko, Wilk and Nusair's local exchange correlation potential was used.[32] Gradient-corrected geometry optimisations[33] were performed by use of the generalised gradient approximation (Becke's exchange[34] and Perdew's correlation[35] functionals). Relativistic effects were treated with the ZORA approximation.[36] The core orbitals were frozen for Os ([1–4]s, [1–4]p, [3–4]d) and C, O (1s). Triple-ζ Slater type orbitals (STOs) were used to describe the valence shells of H (1s), C, O (2s and 2p) and Os (4f, 5d, 6s). A set of two polarisation functions was added: H (single ζ, 2p, 3d), C, O (single ζ, 3d, 4f), Os (single ζ, 6p, 5f). Full geometry optimisations were performed without any symmetry constraints on clusters based on the available crystal structures for the two isomers of cluster $[Os_3(CO)_{10}$(buta-1,3-diene)], with chelate (**2′**) or bridging (**2″**) buta-1,3-diene.[15,16]

The geometry optimisation of the photoproducts $[Os_3(CO)_9(\mu\text{-CO})$(buta-1,3-diene)] (**2a**) and $[Os_3(CO)_8(\mu\text{-CO})_2$(buta-1,3-diene)] (**2b**) started with constraining of the carbonyl groups to remain bridging. After convergence had been achieved, the photoproducts were fully optimised. Various combinations were tried, with one or two CO bridges in several positions. All attempts at full optimisation of the resulting constrained structure of photoproduct **2a** always led to **2b**. The optimised structure **2a** was thus obtained with geometry constraints, while that of **2b** was fully optimised. IR frequencies of the photoproduct **2b** were calculated after full optimisation. A smaller basis set than that described above was used. The core orbitals were frozen for Os ([1–4]s, [1–4]p, [3–4]d, 4f) and C, O (1s). Triple-ζ STOs, plus one polarisation function (single-ζ, 6p), were used to describe the valence shells of Os (5d, 6s). Double-ζ STOs were used to describe the valence shells of H (1s), C and O (2s and 2p). One polarisation function was added to C and O (single-ζ, 3d). As the geometry of **2a** was not completely optimised, frequency calculations were not performed.

Single-point calculations at the DFT/B3LYP[37,38] levels were performed on the ADF-optimised geometries by use of Gaussian 98.[39] This functional includes a mixture of Hartree–Fock exchange with DFT exchange-correlation, given by Becke's three-parameter functional[38] with the Lee, Yang and Parr correlation functional,[37] which includes both local and non-local terms. The standard LanL2DZ basis set was used for Os[40] and a 6–31G* basis set[41] for the other atoms (C, O, H).

A natural population analysis (NPA)[24] was performed and Wiberg indices[23] (using the B3LYP density) were evaluated and used as bond strength indicators. Mayer indices[25] were calculated with the ADF densities by use of the MAYER program.[26]

Time-dependent DFT calculations (TD-DFT)[42] in the ADF implementation were used to determine the excitation energies. In all cases the ten lowest singlet–singlet excitation energies were calculated by use of the optimised geometry.

Acknowledgement

This work was undertaken as a part of the European collaborative COST project (D14/0001/99). Financial support was received by F.W.V. and F.H. from the Council for Chemical Sciences of the Netherlands Organization for Scientific Research (CW-NWO, project No. 348–032) and from the European Union (LSF ref. No. USEV13C2/01). P.J.C. acknowledges FCT for a grant (SFRH/BD/10535/2002).

[1] a) P. Braunstein, J. Rosé in *Comprehensive Organometallic Chemistry, Vol. 10* (Eds.: E. W. Abel, F. Gordon, A. Stone, G. Wilkinson), Pergamon, New York, **1995**, pp. 351–385; b) P. Braunstein, J. Rosé in *Catalysis by Di- and Polynuclear Metal Cluster Complexes* (Eds.: R. D. Adams, F. A. Cotton), Wiley-VCH, New York, **1998**, pp. 443–508.

[2] a) N. E. Leadbeater, *J. Organomet. Chem.* **1999**, *573*, 211–216; b) N. E. Leadbeater, *J. Chem. Soc. Dalton Trans.* **1995**, 2923–2934; c) J. Nijhoff, M. J. Bakker, F. Hartl, D. J. Stufkens, W.-F. Fu, R. van Eldik, *Inorg. Chem.* **1998**, *37*, 661–668; d) A. J. Arce, A. J. Deeming, Y. De Sanctis, D. M. Speel, A. Di Trapani, *J. Organomet. Chem.* **1999**, *580*, 370–377.

[3] E. W. Ainscough, A. M. Brodie, R. K. Coll, T. G. Kotch, A. J. Lees, A. J. A. Mair, J. M. Waters, *J. Organomet. Chem.* **1996**, *517*, 173–181.

[4] a) S. T. Arrivo, T. P. Dougherty, W. T. Grubbs, E. J. Heilweil, *Chem. Phys. Lett.* **1995**, *235*, 247–254; b) T. P. Dougherty, E. J. Heilweil, *Chem. Phys. Lett.* **1994**, *227*, 19–25.

[5] a) M. Poliakoff, J. J. Turner, *Angew. Chem.* **2001**, *113*, 2889–2892; *Angew. Chem. Int. Ed.* **2001**, *40*, 2809–2812; b) P. T. Snee, C. K. Payne, S. D. Mebane, K. T. Kotz, C. B. Harris, *J. Am. Chem. Soc.* **2001**, *123*, 6909–6915.

[6] T. P. Dougherty, E. J. Heilweil, *J. Chem. Phys.* **1994**, *100*, 4006–4009.

[7] T. P. Dougherty, W. T. Grubbs, E. J. Heilweil, *J. Phys. Chem.* **1994**, *98*, 9396–9399.

[8] a) H. Yang, P. T. Snee, K. T. Kotz, C. K. Payne, C. B. Harris, *J. Am. Chem. Soc.* **2001**, *123*, 4204–4210; b) J. C. Owrutsky, A. P. Baronavski, *J. Chem. Phys.* **1996**, *105*, 9864–9873.

[9] F. W. Vergeer, F. Hartl, P. Matousek, D. J. Stufkens, M. Towrie, *Chem. Commun.* **2002**, 1220–1221.

[10] F. W. Vergeer, M. J. Calhorda, P. Matousek, M. Towrie, F. Hartl, *Dalton Trans.* **2003**, 4084–4099.

[11] M. J. Bakker, F. W. Vergeer, F. Hartl, O. S. Jina, X.-Z. Sun, M. W. George, *Inorg. Chim. Acta* **2000**, *300–302*, 597–603.

[12] M. J. Bakker, F. W. Vergeer, F. Hartl, P. Rosa, L. Ricard, P. Le Floch, M. J. Calhorda, *Chem. Eur. J.* **2002**, *8*, 1741–1752.

[13] M. L. Deng, W. K. Leong, *J. Chem. Soc. Dalton Trans.* **2002**, 1020–1023.

[14] a) M. F. Desrossiers, P. C. Ford, *Organometallics* **1982**, *1*, 1715–1716; b) J. Malito, S. Markiewicz, A. Poë, *Inorg. Chem.* **1982**, *21*, 4335–4338.

[15] F.-W. Grevels, W. E. Klotzbücher, J. Schrickel, K. Schaffner, *J. Am. Chem. Soc.* **1994**, *116*, 6229–6237.

[16] M. Tachikawa, J. R. Shapley, R. C. Haltiwanger, C. G. Pierpont, *J. Am. Chem. Soc.* **1976**, *98*, 4651–4652.

[17] C. G. Pierpont, *Inorg. Chem.* **1978**, *17*, 1976–1980.

[18] S. Aime, W. Dastru, R. Gobetto, J. Krause, L. Violano, *Inorg. Chim. Acta* **1995**, *235*, 357–366.

[19] a) M. J. Calhorda, E. Hunstock, L. F. Veiros, F. Hartl, *Eur. J. Inorg. Chem.* **2001**, 223–231; b) E. Hunstock, C. Mealli, M. J. Calhorda, J. Reinhold, *Inorg. Chem.* **1999**, *38*, 5053–5060.

[20] P. C Ford, J. *Organomet. Chem.* **1990**, *383*, 339–356

[21] A. Vlček, Jr., *Coord. Chem. Rev.* **1998**, *171*, 93–105; b) D. J. Stufkens, M. P. Aarnts, J. Nijhoff, B. D. Rossenaar, *Coord.Chem. Rev.* **2000**, *200–202*, 933–978;

[22] F. W. Vergeer, C. J. Kleverlaan, D. J. Stufkens, *Inorg. Chim. Acta* **2002**, *327*, 126–133.

[23] K. B. Wiberg, *Tetrahedron* **1968**, *24*, 1083–1096.

[24] a) J. E. Carpenter, Ph.D. thesis, University of Wisconsin (Madison WI), **1987**; b) J. E. Carpenter, F. Weinhold, *J. Mol. Struct.* **1988**, *169*, 41–62; c) J. P. Foster, F. Weinhold, *J. Am. Chem. Soc.* **1980**, *102*, 7211–7218; d) A. E. Reed, F. Weinhold, *J. Chem. Phys.* **1983**, *78*, 4066–4073; e) A. E. Reed, F. Weinhold, *J. Chem. Phys.* **1985**, *83*, 1736–1740; f) A. E. Reed, R. B. Weinstock, F. Weinhold, *J. Chem. Phys.* **1985**, *83*, 735–746; g) A. E. Reed, L. A. Curtiss, F. Weinhold, *Chem. Rev.* **1988**, *88*, 899–926; h) F. Weinhold, J. E. Carpenter, *The Structure of Small Molecules and Ions*, Plenum, **1988**.

[25] a) I. Mayer, *Chem. Phys. Lett.* 1983, **97**, 270; b) I. Mayer, *Int. J. Quantum Chem.* 1984, **26**, 151.

[26] A. J. Bridgeman, C. J. Empson, MAYER, University of Hull, Hull (UK), **2002**; freely available from the web from http://freeside.dcs.hull.ac.uk/~ch8cje/mayer/index.php.

[27] D. Braga, F. Grepioni, E. Parisini, B. F. G. Johnson, C. M. Martin, J. M. G. Nairn, J. Lewis, M. Martinelli, *J. Chem. Soc. Dalton Trans.* **1993**, 1891–1895.

[28] R. Zoet, J. T. B. H. Jastrzebski, G. van Koten, T. Mahabiersing, K. Vrieze, *Organometallics* **1988**, *7*, 2108–2117.

[29] M. Towrie, D. C. Grills, J. Dyer, J. A. Weinstein, P. Matousek, R. Barton, P. D. Bailey, N. Subramaniam, W. M. Kwok, C. Ma, D. Phillips, A. W. Parker, M. W. George, *Appl. Spectrosc.* **2003**, *57*, 367–380.

[30] R. G. Parr, W. Yang, *Density Functional Theory of Atoms and Molecules*, Oxford University Press, New York, **1989**.

[31] a) E. J. Baerends, A. Bérces, C. Bo, P. M. Boerrigter, L. Cavallo, L. Deng, R. M. Dickson, D. E. Ellis, L. Fan, T. H. Fischer, C. Fonseca - Guerra, S. J. A. van Gisbergen, J. A. Groeneveld, O. V. Gritsenko, F. E. Harris, P. van den Hoek, H. Jacobsen, G. van Kessel, F. Kootstra, E. van Lenthe, V. P. Osinga, P. H. T. Philipsen, D. Post, C. C. Pye, W. Ravenek, P. Ros, P. R. T. Schipper, G. Schreckenbach, J. G. Snijders, M. Sola, D. Swerhone, G. te Velde, P. Vernooijs, L. Versluis, O. Visser, E. van Wezenbeek, G. Wiesenekker, S. K. Wolff, T. K. Woo, T. Ziegler, ADF-2002, Vrije Universiteit, Amsterdam, **2002**; b) E. J. Baerends, D. Ellis, P. Ros, *Chem. Phys.* **1973**, *2*, 41–51; c) E. J. Baerends, P. Ros, *Int. J. Quantum Chem.* **1978**, *S12*, 169–190; d) P. M. Boerrigter, G. te Velde, E. J. Baerends, *Int. J. Quantum Chem.* **1988**, *33*, 87–113; e) G. te Velde, E. J. Baerends, *J. Comput. Phys.* **1992**, *99*, 84–98.

[32] S. H. Vosko, L. Wilk, M. Nusair, *Can. J. Phys.* **1980**, *58*, 1200–1211.

[33] a)L. Fan, T. Ziegler, *J. Chem. Phys.* **1991**, *95*, 7401–7408; b) L. Versluis, T. Ziegler, *J. Chem. Phys.* **1988**, *88*, 322–328.

[34] A. D. Becke, *J. Chem. Phys.* **1988**, *88*, 1053–1062.

[35] J. P. Perdew, *Phys. Rev. B* **1986**, *33*, 8822–8824; b) J. P. Perdew, *Phys. Rev. B* **1986**, *34*, 7406.

[36] E. van Lenthe, A. Ehlers, E. J. Baerends, *J. Chem. Phys.* **1999**, *110*, 8943–8953.

[37] C. Lee, W. Yang, R. G. Parr, *Phys. Rev. B* **1988**, *37*, 785–789.

[38] A. D. Becke, *J. Chem. Phys.* **1993**, *98*, 5648–5652.

[39] Gaussian 98 (Revision A.7), M. J. Frisch, G. W. Trucks, H. B. Schlegel, G. E. Scuseria, M. A. Robb, J. R. Cheeseman, V. G. Zakrzewski, J. A. Montgomery, Jr., R. E. Stratmann, J. C. Burant, S. Dapprich, J. M. Millam, A. D. Daniels, K. N. Kudin, M. C. Strain, O. Farkas, J. Tomasi, V. Barone, M. Cossi, R. Cammi, B. Mennucci, C. Pomelli, C. Adamo, S. Clifford, J. Ochterski, G. A. Petersson, P. Y. Ayala, Q. Cui, K. Morokuma, D. K. Malick, A. D. Rabuck, K. Raghavachari, J. B. Foresman, J. Cioslowski, J. V. Ortiz, B. B. Stefanov, G. Liu, A. Liashenko, P. Piskorz, I. Komaromi, R. Gomperts, R. L. Martin, D. J. Fox, T. Keith, M. A. Al-Laham, C. Y. Peng, A. Nanayakkara, C. Gonzalez, M. Challacombe, P. M. W. Gill, B. G. Johnson, W. Chen, M. W. Wong, J. L. Andres, M. Head-Gordon, E. S. Replogle, J. A. Pople, Gaussian, Inc., Pittsburgh, PA, **1998**.

[40] a) T. H. Dunning, Jr., P. J. Hay in *Modern Theoretical Chemistry, Vol. 3* (Ed.: H. F. Shaefer, III), Plenum Press, New York, **1977**, pp. 1–27; b) P. J. Hay, W. R. Wadt, *J. Chem. Phys.* **1985**, *82*, 270–283; c) P. J. Hay, W. R. Wadt, *J. Chem. Phys.* **1985**, *82*, 299–310.

[41] a) R. Ditchfield, W. J. Hehre, J. A. Pople, *J. Chem. Phys.* **1971**, *54*, 724–728; b) W. J. Hehre, J. A. Ditchfield, J. A. Pople, *J. Chem. Phys.* **1972**, *56*, 2257–2261; c) P. C. Hariharan, J. A. Pople, *Theor. Chim. Acta* **1973**, *28*, 213–222; d) P. C. Hariharan, J. A. Pople, *Mol. Phys.* **1974**, *27*, 209–214; e) M. S. Gordon, *Chem. Phys. Lett.* **1980**, *76*, 163–168.

[42] a) S. J. A. van Gisbergen, J. A. Groeneveld, A. Rosa, J. G. Snijders, E. J. Baerends, *J. Phys. Chem. A* **1999**, *103*, 6835–6844; b) A. Rosa, E. J. Baerends, S. J. A. van Gisbergen, E. van Lenthe, J. A. Groeneveld, J. G. Snijders, *J. Am. Chem. Soc.* **1999**, *121*, 10356–10365; c) S. J. A. van Gisbergen, A. Rosa, G. Ricciardi, E. J. Baerends, *J. Chem. Phys.* **1999**, *111*, 2499–2506.

Received: January 26, 2004
Published online: May 25, 2004

